Decomposition Pathways of Hydrotalcite-like Compounds $Mg_{1-x}Al_x(OH)_2(NO_3)_x \cdot nH_2O$ as a Continuous Function of Nitrate Anions

Z. P. Xu and H. C. Zeng*

Department of Chemical and Environmental Engineering, Faculty of Engineering, National University of Singapore, 10 Kent Ridge Crescent, Singapore 119260

Received April 23, 2001. Revised Manuscript Received August 8, 2001

Thermal decomposition pathways of our recently prepared hydrotalcite-like compounds $Mg_{1-x}Al_x(OH)_2(NO_3)_x \cdot nH_2O$ in $x = 0.20-0.34$ (*J. Phys. Chem. B* **2001**, *105*, 1743−1749) have been investigated with XRD, DTA, TGA, FTIR, and combined TGA/FTIR techniques. It has been found that, unlike those in carbonated hydrotalcites, the dehydroxylation and decomposition of anions in low nitrate-content (x) hydrotalcites are separated, while the two processes in the high x samples are overlapped. In line with our recent structural models, the dehydroxylation process in the samples with high x value can be further differentiated into steps, depending on chemical nature of hydroxyl group and nitrate content. The layered structure of these hydrotalcite compounds becomes thermally more stable when more nitrate ions are intercalated. The depletion of nitrate anions (decomposed into NO_2 and O_2) in the low x compounds is a continuous process, whereas that in the high x compounds is a discrete one. At 400 °C, most nitrate anions are still retained in the interlayer space with both D_{3h} and C_{2v} symmetries, although the dehydroxylation reaction in the low x samples is largely completed. At 500 °C, intercalated nitrate anions are mostly decomposed and the remaining ones are mainly in C_{2v} symmetry with a standing configuration between two dehydroxylated brucite-like layers. The nearest distance between two oxygen octahedrons changes from 3.088 to 3.040 Å to 2.99−2.97 Å when the hydrotalcite-like phase is topotactically transformed to a rock-salt-like phase.

Introduction

Hydrotalcite-like compounds (HTlcs), also known as layered double hydroxides (LDHs), have received extensive research in recent years.[1−8] Interests in such materials rest not only in their potential catalytic applications in many chemical reactions but also in many separation, transport, and materials applications, such as anion adsorbents, anion exchangers, scavengers, gene delivery vectors, and medicine and polymer stabilizers.[1−8]

In the brucite-like compounds, a divalent metal cation is located in the center of oxygen octahedron constructed by six hydroxyl groups. The resultant octahedrons are connected with one another by edge-sharing to form two-dimensionally infinite layers, which is similar to the basic structure of brucite $Mg(OH)_2$.[1] The brucite-like layers can stack upon one another owing to various chemical interactions between the layers. Substitution of trivalent cations for some divalent ones in the brucite layers causes organic or inorganic anions to be intercalated into the space between brucite-like layers (interlayer space) thus leading to the formation of hydrotalcite-like structure that is restricted to particular M^{2+}/M^{3+} combinations as in mineral $Mg_6Al_2(OH)_{16}CO_3 \cdot 4H_2O$.[1b]

It is well-known that using the coprecipitation method trivalent and divalent cations are very evenly distributed in the brucite-like layers, thermal decomposition of which will lead to the formation of well-mixed multimetal oxide materials.[9] Since physicochemical properties of ultimate calcined HTlcs are greatly influenced by the thermal decomposition procedure used, numerous studies of the thermal stability of various carbonated $Mg_{1-x}Al_x$-CO_3-HTlcs have been reported.[1,10−20] For example, thermal decomposition of $Mg_{1-x}Al_x$-CO_3-

* To whom correspondence should be addressed. Tel: +65 874 2896. Fax: +65 779 1936. E-mail: chezhc@nus.edu.sg.

(1) (a) Cavani, F.; Trifiro, F.; Vaccari, A. *Catal. Today* **1991**, *11*, 173. (b) Allmann, R. *Acta Crystallogr.* **1968**, *B24*, 972. (c) Taylor, H. F. W. *Miner. Magn.* **1969**, *37*, 338.

(2) Reiche, W. T. *Solid State Ionics* **1986**, *22*, 133.

(3) Faure, C.; Borthomieu, Y.; Delmas, C.; Fonsassier, M. *J. Power Sources* **1991**, *36*, 113.

(4) Armor, J. N.; Braymer, T. A.; Farris, T. S.; Li, Y.; Petrocelli, F. P.; Weist, E. L.; Kannan, S.; Swamy, C. S. *Appl. Catal. B* **1996**, *7*, 397.

(5) Hermosin, M. C.; Pavlovic, J.; Ulibarri, M. A.; Cornejo, J. *Water Res.* **1996**, *30*, 171.

(6) Chisem, I. C.; Jones, W. *J. Mater. Chem.* **1994**, *4*, 1737.

(7) (a) Choy, J. H.; Kwak, S. Y.; Park, J. S.; Jeong, Y. J.; Portier, J. *J. Am. Chem. Soc.* **1999**, *121*, 1399. (b) Choy, J. H.; Kwak, S. Y.; Jeong, Y. J.; Park, J. S. *Angew. Chem. Int. Ed.* **2000**, *39*, 4042.

(8) (a) Qian, M.; Zeng, H. C. *J. Mater. Chem.* **1997**, *7*, 493. (b) Xu, Z. P.; Zeng, H. C. *Chem. Mater.* **1999**, *11*, 67. (c) Xu, Z. P.; Zeng, H. C. *J. Mater. Chem.* **1998**, *8*, 2499.

(9) Markov, L.; Petrov, K.; Lyubchova, A. *Solid State Ionics* **1990**, *39*, 187.

(10) Pesic, L.; Salipurovic, S.; Markovic, V.; Vucelic, D.; Kagunya, W.; Jones, W. *J. Mater. Chem.* **1992**, *2*, 1069.

(11) Tsuji, M.; Mao, G.; Yoshida, T.; Tamaura, Y. *J. Mater. Res.* **1993**, *8*, 1137.

(12) Rey, F.; Fornes, V.; Rojo, J. M. *J. Chem. Soc., Faraday Trans.* **1992**, *88*, 2233.

10.1021/cm010347g CCC: $20.00
Published on Web 10/12/2001

Table 1. Elemental Analyses and Chemical Formulas of the Studied $Mg_{1-x}Al_x$-NO_3-HTlcs

sample	x_{ini}[a]	x[b]	A/M[c]	Mg %[d]	Al %[d]	N %[d]	C %[d]	chemical formula
MA1	0.167	0.20	0.22	22.5	6.1	3.1	0.16	$Mg_{0.80}Al_{0.20}(OH)_{1.98}(NO_3)_{0.19}(CO_3)_{0.015} \cdot 0.9H_2O$
MA2	0.20	0.22	0.23	22.0	6.9	3.4	0.16	$Mg_{0.78}Al_{0.22}(OH)_{1.99}(NO_3)_{0.20}(CO_3)_{0.015} \cdot 0.8H_2O$
MA3	0.25	0.26	0.25	22.0	8.8	4.16	0.08	$Mg_{0.74}Al_{0.26}(OH)_{2.01}(NO_3)_{0.24}(CO_3)_{0.005} \cdot 0.4H_2O$
MA4	0.30	0.31	0.31	20.0	10.2	5.04	0.08	$Mg_{0.69}Al_{0.31}(OH)_{2.00}(NO_3)_{0.30}(CO_3)_{0.005} \cdot 0.3H_2O$
MA5	0.33	0.34	0.33	29.0	10.7	5.12	0.16	$Mg_{0.66}Al_{0.34}(OH)_{2.00}(NO_3)_{0.31}(CO_3)_{0.01} \cdot 0.3H_2O$

[a] x_{ini} is the initial molar ratio [Al]/([Al] + [Mg]) in the metal cation solution. [b] x is the molar ratio [Al]/([Al] + [Mg]) found in the precipitate. [c] A/M is the molar ratio ($[NO_3^-] + 2[CO_3^{2-}]$)/([Al] + [Mg]) in the precipitate. [d] The percentage is in weight.

HTlcs has been studied in detail with many techniques, such as TG/MS,[10] TG/IR,[21] TG/DTA/MS,[11] NMR,[12] and SEM/TEM.[13] It has been found that the release of CO_2 generally spans a wide temperature range but sometimes undergoes two different stages and generally overlaps with dehydroxylation process.[1,10,11] Nevertheless, thermal decomposition of nitrated $Mg_{1-x}Al_x$-NO_3-HTlcs has yet to be investigated in the same depth and scope as in $Mg_{1-x}Al_x$-CO_3-HTlcs.[22−24] In this regard, we have recently investigated the nitrated $Mg_{1-x}Al_x$-NO_3-HTlcs and found that nitrated $Mg_{1-x}Al_x$-NO_3-HTlcs have different anionic arrangements from that of the carbonated ones in the interlayer space.[1,24−26] More importantly, due to different chemical natures of nitrogen and carbon in NO_3^- and CO_3^{2-}, the decomposition of NO_3^- will involve the change of oxidation states of nitrogen, whereas that of CO_3^{2-} does not. It is anticipated that nitrated $Mg_{1-x}Al_x$-NO_3-HTlcs will show different thermal decomposition pathways, which may further affect a final topotactic transformation of brucite-like layers into a rock-salt-like phase (or Al_2O_3-doped MgO) because of variations in cation ratio and anion number. From the environmental prospect, furthermore, a detailed understanding on nitrate anion decomposition in the LDHs may shed lights on nitrogen oxide management and recycle. For example, intercalation of nitrate anions in the solid LDHs may provides us a new means for nitrate anion removal or recovery, because most metal nitrates are highly soluble in aqueous solutions. On the other hand, thermal decomposition of nitrated LDHs will release gaseous nitrogen oxides, such as NO_2 produced in the current experiments, which can then be directly absorbed in water to form nitric acid.[27]

To understand the general thermal processes of the nitrated HTlcs upon heat treatments, we report here a detailed investigation of the thermal and structural evolutions of a series of $Mg_{1-x}Al_x$-NO_3-HTlcs with trivalent cation content (x) from 0.20 to 0.34. In particular, dehydration, dehydroxylation, and release patterns of H_2O and NO_2 (i.e., decomposition of intercalated NO_3^-) have been on-line monitored with a TGA/FTIR technique, and transformation of the as-prepared $Mg_{1-x}Al_x$-NO_3-HTlcs to final mixed oxides has been also examined in detail with TGA, DTA, CHN/ICP, XRD, and FTIR methods.

Experimental Section

Sample Preparation. A coprecipitation method was used to prepare $Mg_{1-x}Al_x$-NO_3-HTlcs.[26] Briefly, 20.0 mL of salt solution containing $Mg(NO_3)_2 \cdot 6H_2O$ (Merck, 99%) and $Al(NO_3)_3 \cdot 9H_2O$ (Merck, 98.5%) was added dropwise within 10 min into a rigorously stirred ammoniacal solution (100.0 mL, 0.5 M, at room temperature) which was bubbled for 15 min with purified air (40 mL min^{-1}) prior to the addition of cation solutions. The total cation concentration was kept at 1.0 M for the syntheses of all five samples, while the molar ratio of cations $[Al^{3+}]/([Mg^{2+}] + [Al^{3+}])$ was varied as listed in Table 1. The sample names (from MA1 to MA5) are designated sequentially according to the content of trivalent cation Al^{3+}. After aging at 65 °C for 18 h, the solid−solution mixture was then filtered and washed thoroughly with deionized water, followed by a drying overnight in vacuo at room temperature.

Characterization Techniques. Crystallographic information on the samples was investigated by powder X-ray diffraction (XRD).[26] Chemical bonding information on metal−oxygen, hydroxyl, and intercalated anion (such as NO_3-) was collected with Fourier transform infrared spectroscopy (FTIR).[26] Carbon and nitrogen contents of the as-prepared $Mg_{1-x}Al_x$-NO_3-HTlcs were determined by CHN-analysis, while the magnesium and aluminum contents were measured by inductively coupled plasma (ICP) emission spectroscopy.[26]

Studies with both differential thermal analysis (DTA, Shimadzu DTA-50) and thermogravimetric analysis (TGA, Shimadzu TGA-50) were carried out to understand thermal behaviors of the prepared samples. In each measurement, ca. 15 mg of sample was heated at a rate of 10 °C min^{-1} with a flow of air at 40 mL min^{-1} over the temperature range of 40−800 °C. For a further comparison, the differential TGA (DrTGA) curves were derived accordingly.

In combined TGA/FTIR investigation (TGA 2050, TA Instruments/FTIR, Bio-Rad, Model FTS 3500), the gases evolved from the $Mg_{1-x}Al_x$-NO_3-HTlc sample heated with TGA (at a rate of 10 °C min^{-1}) were introduced

(13) Valchevatraykova, M. L.; Davidova, N. P.; Weiss, A. H. *J. Mater. Sci.* **1993**, *28*, 2157.
(14) Marino, O.; Mascolo, G. *Proc. 2nd Euro. Symp. Thermal Anal.* **1981**, 391.
(15) Labajos, F. M.; Rives, V.; Ulibarri, M. A. *J. Mater. Sci.* **1992**, *27*, 1546.
(16) del Arco, M.; Trujillano, R.; Rives, V. *J. Mater. Chem.* **1998**, *8*, 761.
(17) Labajos, F. M.; Rives, V. *Inorg. Chem.* **1996**, *35*, 5313.
(18) Hibino, T.; Kosuge, K.; Tsunashima, A. *Clays Clay Miner.* **1996**, *44*, 151.
(19) Sato, T.; Fujita, H.; Endo, T.; Shimada, M. *React. Solids* **1988**, *5*, 219.
(20) Miyata, S. *Clays Clay Mater.* **1980**, *28*, 50.
(21) (a) Bellotto, M.; Rebours, B.; Clause, O.; Lynch, J.; Bazin, D.; Elkaim, E. *J. Phys. Chem.* **1996**, *100*, 8527. (b) Bellotto, M.; Rebours, B.; Clause, O.; Lynch, J.; Bazin, D.; Elkaim, E. *J. Phys. Chem.* **1996**, *100*, 8535.
(22) Del Arco, M.; Gutierrez, S.; Martin, C.; Rives, V.; Rocha, J. *J. Solid State Chem.* **2000**, *151*, 272.
(23) Kooli, F.; Chisem, I. C.; Vucelic, M.; Jones, W. *Chem. Mater.* **1996**, *8*, 1969.
(24) Kruissink, E. C.; van Reijen, L. L.; Ross, J. R. H. *J. Chem. Soc., Faraday Trans. 1* **1981**, *77*, 649.
(25) Miyata, S. *Clays Clay Miner.* **1983,** *31*, 305.
(26) Xu; Z. P.; Zeng, H. C. *J. Phys. Chem. B* **2001**, *105*, 1743.
(27) Cotton, F. A.; Wilkinson, G. *Advanced Inorganic Chemistry*; John Willey & Sons: New York, 1980; Chapter 13, p 416.

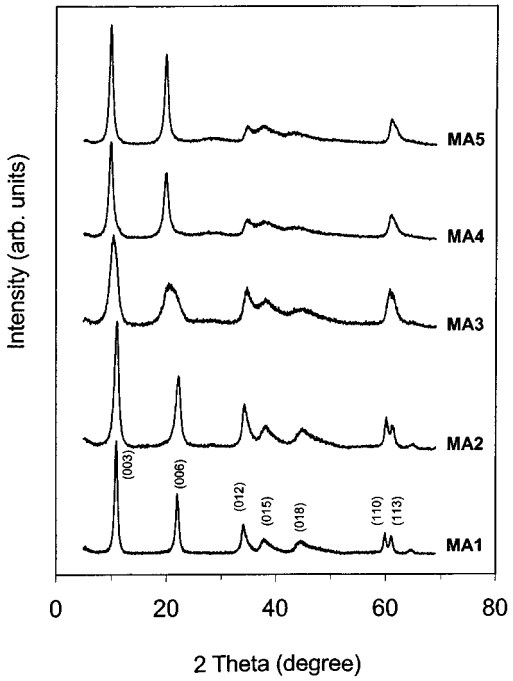

Figure 1. XRD patterns of the as-prepared hydrotalcite-like samples MA1−MA5.

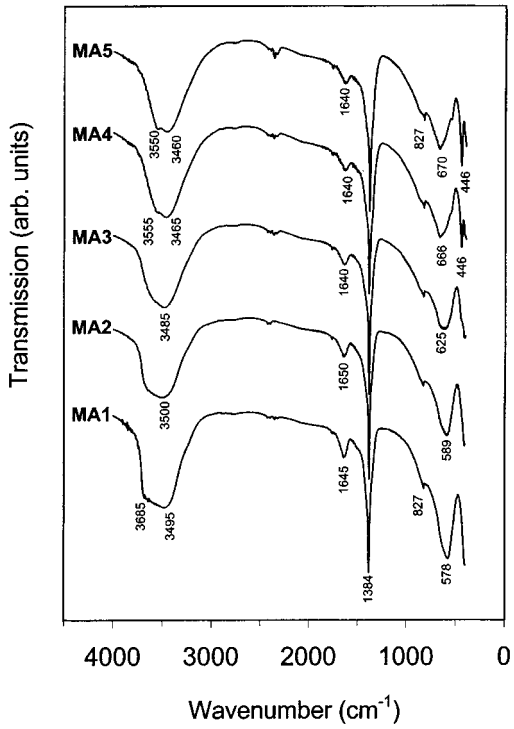

Figure 2. FTIR spectra of the as-prepared hydrotalcite-like samples MA1−MA5.

into a measurement cell by carrier gas (air at a rate of 100 mL min^{-1}), and then a series of FTIR spectra were recorded in about every 4 s. To monitor the infrared absorbance changes versus time, i.e., versus the temperature of TGA, The Gram-Schmidt reconstruction technique was used to construct the chromatogram from the collected set of interferograms.[28,29] This chromatogram is essentially a measure of the integrated absorbance in each spectrum versus time. Especially for the decomposed species, such as H_2O, CO_2 and NO_2 that have their own characteristic vibrational modes, the infrared-based chromatograms were also created by integrating the absorbance in a specified wavenumber region of the actual absorbance in IR spectra. In this work, the chromatograms for the major gaseous molecules of H_2O (3850−3857 cm^{-1}) and NO_2 (2915−2930 cm^{-1}) were created. The deduced chromatograms were taken as the changes of the relative concentration of the evolved gaseous species versus time or temperature.

Results and Discussion

Structural and Compositional Analysis. Table 1 summarizes the results of elemental analyses.[26] The X-ray diffraction patterns of the as-prepared samples are shown in Figure 1, which confirms the formation of hydrotalcite-like structure in all compounds.[1,30] It is observed that the (003) and (006) peaks shift to smaller 2θ angles when the x value is increased in the sequence from MA1 to MA5. The abrupt increase in the basal spacing (8.08 to 8.95 Å) through MA3 had been attributed to different arrangements of NO_3^- anions in the interlayer space, as discussed in an our previous paper.[26] Two models for the NO_3^- arrangement had been proposed: (i) When the x value is low, the anions adopt a flat-lying configuration, similar to divalent CO_3^{2-} in the normal hydrotalcite. (ii) When x reaches a threshold value (MA3), the planar NO_3^- anions adjust their flat-lying style and stick up and down alternatively to the two adjacent brucite-like layers.[26] The stick-lying configuration of NO_3^- anions and thus larger basal spacing are due to higher repulsion among the anions when their population in interlayer space is increased.

The changes of FTIR spectra of the as-prepared samples are presented in Figure 2. The most prominent feature for this spectral evolution is that there is an intensive sharp peak at 1384 cm^{-1} (assigned to ν_3 vibrational mode of NO_3^- with D_{3h} symmetry) that shows no peak shift. Similarly, a weak peak at 827 cm^{-1} caused by the ν_2 mode of the same anion also shows no shift in all the IR spectra.[6,7,10,31−36] The constant wavenumbers of these two modes have indicated that nitrate anions intercalated in either larger or smaller interlayer space are relatively unperturbed, keeping their D_{3h} symmetry unchanged.[26] Another important support for our models is the change of ν_{OH} stretching vibration at around 3500 cm^{-1}. It is noted that the broad OH

(28) Griffiths; P. R.; de Haseth, J. A. *Fourier Transform Infrared Spectrometry, Chemical Analysis;* Wiley-Interscience: New York, 1986; Vol. 83.
(29) Akinade, K. A.; Campbell, R. M.; Compton, D. A. C. *J. Mater. Sci.* **1994**, *29*, 3802.
(30) Kuma, K.; Paplawsky, W.; Gedulin, B.; Arrhenius, G. *Origins Life Evol. Biosphere* **1989**, *19*, 573.
(31) Newman, S. P.; Jones, W. *J. Solid State Chem.* **1999**, *148*, 26.
(32) (a) Delahaye-Vidal, A.; Ehlsissen, K. T.; Genin, P.; Figlarz, M. *Eur. J. Solid State Inorg. Chem.* **1994**, *31*, 823. (b) Ehlsissen, K. T., Delahaye-Vidal, A.; Genin, P.; Figlarz, M.; Willmann, P. *J. Mater. Chem.* **1993,** *3*, 883.
(33) Rajamathi, M.; Kamath, P. V.; Seshadri, R. *Mater. Res. Bull.* **2000**, *35*, 271.
(34) Faure, C.; Delmas, C.; Willmann, P. *J. Power Sources* **1991**, *36*, 497.
(35) Gadsden, J. A. *Infrared Spectra of Minerals and Related Inorganic Compounds*; Butterworth: London, 1975; pp 21−24.
(36) Nakamoto, K. *Infrared and Raman Spectra of Inorganic and Coordination Compounds*; Part A, 5th ed; John Wiley and Sons: New York, 1997.

vibration band is resolved more clearly into two components when x exceeds 0.26 (MA3, Table 1), which had been attributed to the change of NO_3^- arrangement.[26] According to the proposed stick-lying model, the hydroxyl groups stuck with NO_3^- anions will exhibit low wavenumber (i.e., 3460−3465 cm^{-1}) due to the O−H bond electron density lowering,[15] while the unstuck hydroxyls show high values (i.e., 3550−3555 cm^{-1} in MA4 and MA5). Furthermore, the δ-mode of O−H groups jumps from 578 to 589 to 666−670 cm^{-1} with a transition point at 625 cm^{-1} (MA3) when the aluminum content in the brucite-like layers is increased. The gradual decrease in intensity of the peak at 1650−1640 cm^{-1} (δ_{HOH} mode of water molecules[12,17]) is in good agreement with the decrease of water content from samples MA1−MA5 (see chemical formulas, Table 1). In addition, lattice vibrations of metal−oxygen bonds are also observed at 550 cm^{-1} (unmarked in the spectra of MA4 and MA5) and 446 cm^{-1} or lower (in MA1−MA3).[15,37]

Thermal Decomposition Behaviors. The DTA curves of MA1−MA5 are reported in Figure 3a. In general, there are two major endothermic events during the compound decomposition. The first band at 124−135 °C is due to the removal of water molecules from the interlayer space, showing a similar interaction of the water molecules with their surrounding chemical species, such as the intercalated anions and OH groups of the brucite-like layers. It should be mentioned that there is no endothermic peak at around 260 °C, which had been reported in the literature for the removal of strongly bonded water molecules, e.g., in the hydrotalcite compound of $Mg_{1-x}Al_x$-CO_3-HT.[1,14] The second one, starting at 250−300 °C, is much broader, especially for samples MA4 and MA5. Noticeably, this thermal event shifts from 355 to 380 to 456−433 °C with the increase of x values from 0.20 to 0.34. The overall increase in decomposition temperature indicates an increase of thermal stability for these compounds.[22,23] This observation is rather different from that in the study of Mg_{1-x}-Al_x-CO_3-HT, which shows a decrease in decomposition temperature from ca. 430 to ca. 400 °C when x increases from 0.20 to 0.34.[1,15,20] It can also be noted that there are some endothermic shoulders on both sides of the band maximums, being more pronounced in samples MA3−MA5. The endothermic band, consisting of many steps, includes collapse of the layer structure and depletion of NO_3^- anions. More definite assignments of these thermal steps will be carried out with the combined TGA/FTIR technique, as will be presented shortly.

Similarly, differential TGA (DrTGA; Figure 3b) profiles from these samples also reflect the above two major endothermic events. Moreover, a third thermal event is resolved at around 475−500 °C as a hump or shoulder on the high-temperature side. The positions and shapes of DrTGA peaks from samples MA1 (x = 0.20) and MA3 (x = 0.26) are quite similar to those reported for the low-nitrate-content $Mg_{1-x}Al_x$-NO_3-HT under similar decomposition conditions.[23] As listed in Table 2, the measured weight loss data are in good agreement with those estimated from the chemical formulas for samples MA3−MA5 (i.e., theoretical weight loss), showing an almost complete decomposition at 650 °C. Nonetheless, the measured weight loss percentages for samples MA1 and MA2 are less than the estimated values by 3−5% (Table 2). The small discrepancy is mainly due to the removal of the weakly adsorbed water in the samples with air flushing before starting the TGA measurement

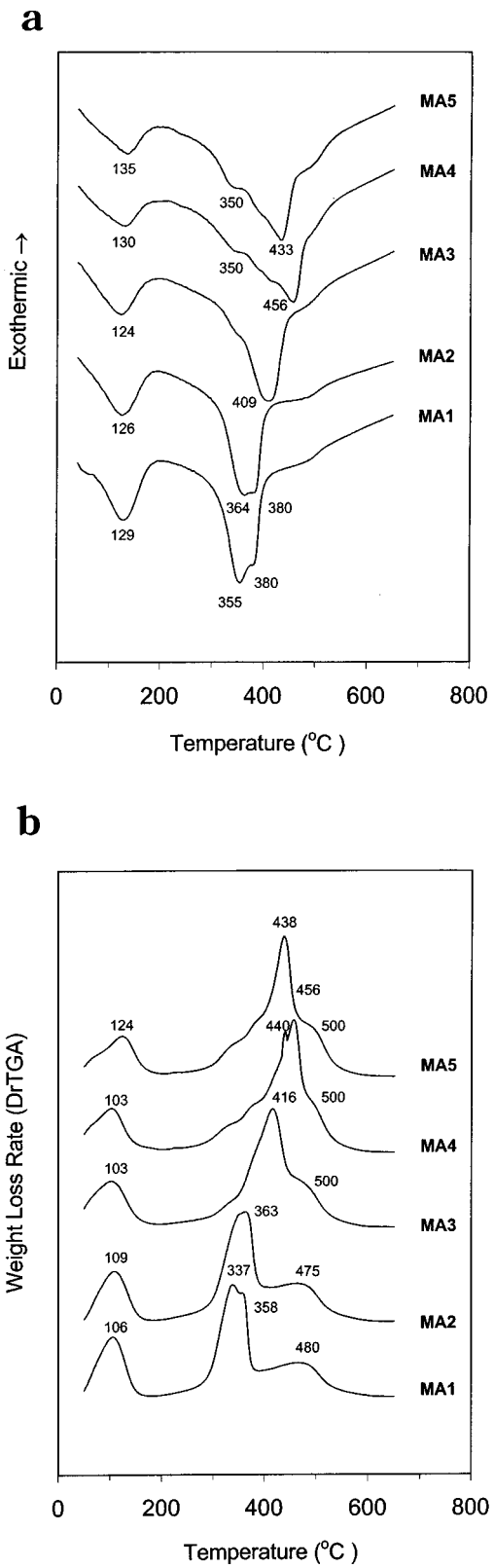

Figure 3. Decomposition of the as-prepared MA1−MA5 samples in air: (a) DTA scans and (b) DrTGA curves (heating rate: 10 °C min^{-1}; flow-rate: 40 mL min^{-1}).

(37) Kannan, S.; Velu, S.; Ramkumar, V.; Swamy, C. S. *J. Mater. Sci.* **1995**, *30*, 1462.

Table 2. Weight Loss Data (%) of the Studied $Mg_{1-x}Al_x$-NO_3-HTlcs

	experimental		theoretical	
sample	200 °C	650 °C	dehydration	total weight loss
MA1	13.5	49.8	17.0	55.5
MA2	13.5	47.8	16.5	50.8
MA3	8.6	46.8	8.8	47.2
MA4	7.5	48.5	6.5	47.7
MA5	7.0	48.5	6.4	48.2

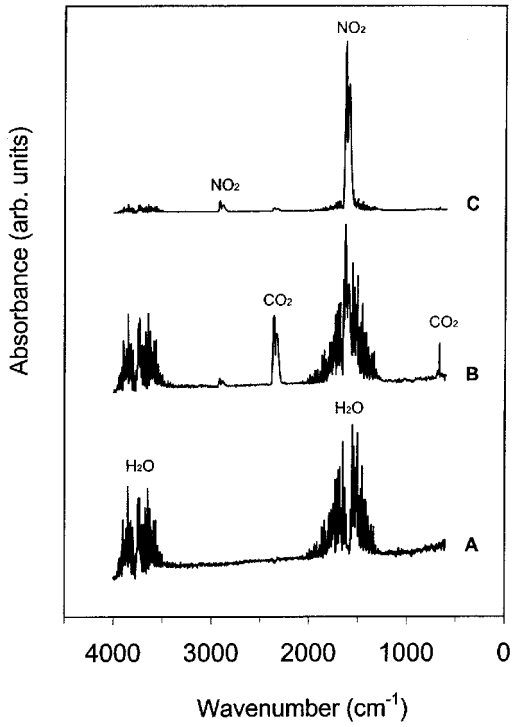

Figure 4. Representative FTIR spectra of evolved gases from sample MA5 at different TGA temperatures. A, 115 °C; B, 400 °C; and C, 455 °C (refer also to MA5 in Figure 5).

(i.e., the zero-setting),[10] which indicates that the "dry" samples of MA1 and MA2 indeed have high hydration ability as revealed in Figure 2.

Dehydration and Dehydroxylation. Figure 4 displays three representative FTIR spectra recorded at 115, 400, and 455 °C upon heating MA5. The bands at 3850−3857 and 2915−2930 cm^{-1} are chosen to represent H_2O and NO_2, respectively.[36,38] The integration of absorbance within the above wavenumber range is thus proportional to the concentration of a chemical species in the gas mixture at that temperature, and thus the change of the integration (i.e., chromatogram) shows the evolution profile of the gaseous species with heating temperature in TGA. Since the release pattern of CO_2 from HTlcs has been relatively clear in the reported literature[10−12] and our samples contain only a trace amount of CO_3^{2-} (Table 1), we do not pursue further examination on CO_2 evolution in this work.

The chromatograms of gaseous water for all samples are shown in Figure 5a. Two major steps, dehydration at 114−120 °C and dehydroxylation at 335−460 °C, can be clearly observed, which further excludes the existence of strongly bonded water at around 260 °C as mentioned ealier.[1,14] The peak contours and positions of these H_2O chromatograms (Figure 5a) are mirroring essentially those of the DTA curves (Figure 3a), revealing that the endothermic heat fluxes in DTA are mainly due to the dehydration and dehydroxylation processes. As the x value increases, the second thermal process (dehydroxylation) moves toward higher temperatures, approximately from 350 to 370 to 417−460 °C. This has further

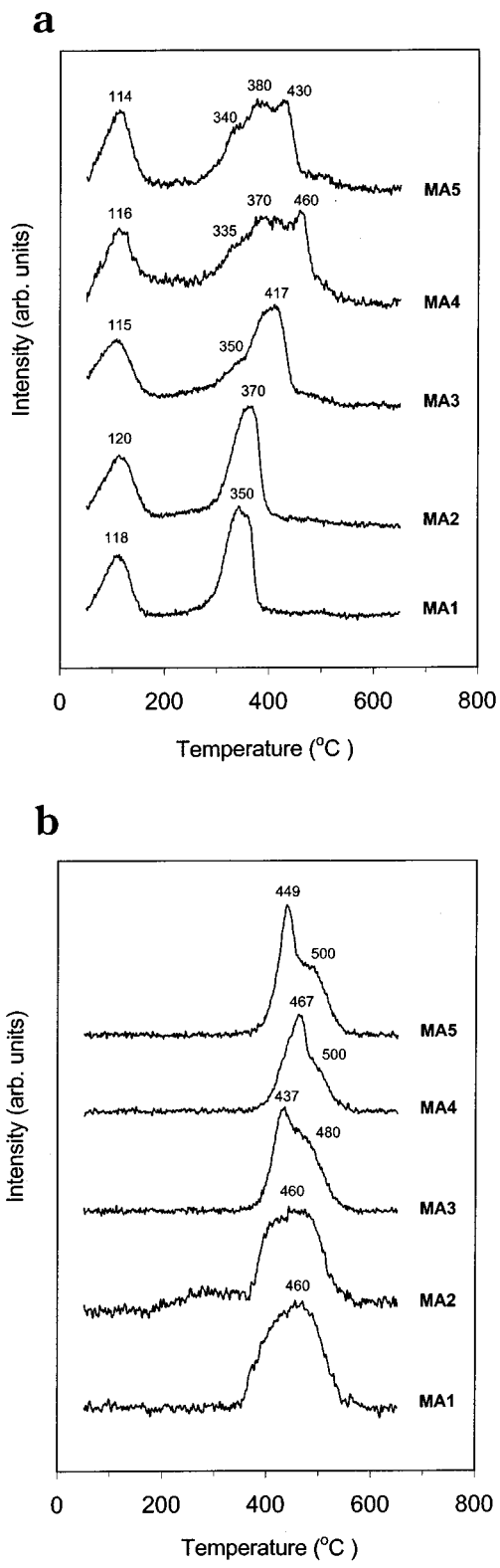

Figure 5. Chromatograms of (a) gaseous H_2O and (b) NO_2 in the combined TGA/FTIR measurements for samples MA1−MA5 with air as carrier gas (heating rate, 10 °C min^{-1}; flow-rate, 100 mL min^{-1}).

(38) Pouchert, C. J. Ed. *The Aldrich Library of FT-IR Spectra*; Aldrich Chemical Co.: US, 1985.

shown that the layered structure of HTlcs becomes thermally more stable when more trivalent Al^{3+} cations are incorporated into the brucite-like layers. However, as reported in the literature, dehydroxylation of $Mg_{1-x}Al_x$-OH-HTlcs (for $x = 0.24-0.33$) occurs over a very narrow temperature range of ca. 420−430 °C.[39] It is thus believed that the stabilization effect, or the destabilization effect, must be related to the intercalated anions as well.

According to the dehydroxylation profiles (Figure 5a), the samples under study may experience different decomposition pathways. For example, samples MA1 and MA2 collapse rapidly within a narrow temperature range of ca. 100 deg (i.e., 300−400 °C), while samples MA4 and MA5 decompose over a larger range of ca. 200 deg (i.e., 300−500 °C), noting that MA3 is an intermediate case (Figure 5a). For the long-lasting cases of MA4 and MA5, three smaller steps can be further differentiated. The differences observed in dehydroxylation may be brought up by their arrangements of the intercalated anions.[26] In the "flat-lying" structure (MA1 and MA2), the hydroxyl groups in the brucite-like layers are more similar, which may result in a one-step decomposition behavior probably due to a monomolecular decomposition of the nitrate anions. However, the alternative "stick-lying" of NO_3^- anions creates different types of hydroxyl groups in the brucite-like layers (MA3-MA5),[26] which could complicate the dehydroxylation. Furthermore, considering that more Al^{3+} ions are incorporated ($x = 0.26-0.34$),[1,18,40] we might conceive more separate steps of dehydroxylation (Figure 5a).

Decomposition of Nitrate Anions. The release of NO_2, i.e., an indication of decomposition of NO_3^- in the interlayer space, is recorded versus heating temperature in Figure 5b. Unlike in a reported TG/IR investigation for $Mg_{1-x}Al_x$-CO_3-HTlcs,[21] which showed that release patterns for both H_2O and CO_2 are identical, the release pattern of NO_2 in our $Mg_{1-x}Al_x$-NO_3-HTlcs are substantially different from that of H_2O. Obviously, the intercalated nitrate anions decompose in the temperature range 360−540 °C, with the band position being relatively unchanged at around 460 °C. The broad band for samples MA1 and MA2 shows that the depletion of intercalated NO_3^- is a continuous process. However, samples MA3, MA4, and MA5 undergo a quick NO_2 release at 437, 467, and 449 °C, which is then followed by a shoulder at 480, 500, and 500 °C, respectively. This observation indicates that there are two distinguishable processes, although they are overlapped. The two release stages of NO_2 are also observed in the decompositions of $Co_{1-x}^{II}Co_x^{III}$-NO_3-HTlcs[41] as well as of several transition metal nitrates.[4242] Interestingly, some carbonated HTlcs, e.g., $Zn_{1-x}Al_x$-CO_3-HTlc and $Cu_{1-x}Al_x$-CO_3-HTlc, have also shown two similar release stages of CO_2 during the decomposition.[11] A further discussion on the release patterns of NO_2 will be given in a later subsection.

In view of the decomposition order, dehydroxylation has been largely completed prior to the depletion of NO_3^- for samples MA1 and MA2, while these two thermal processes are partially overlapped for samples MA3, MA4, and MA5. These observations provide us with answers to (refer to DrTGA curves in Figure 3b) (i) why there is an intense band at 337−363 °C (dehydroxylation) and a broad one at 400−500 °C (depletion of NO_3^-) for MA1 and MA2 and (ii) why there is a strong sharp peak at 416−456 °C (due to both dehydroxylation and depletion of NO_3^-) with a shoulder at around 500 °C (largely due to depletion of NO_3^-) for MA3−MA5. Similar explanation could also be applied to address the combined heat fluxes in DTA measurements (Figure 3a).

Condensation of Layered Structures. To monitor the layered structure change, the samples MA3, MA4, and MA5 were heated from room temperature to 300, 400, and 500 °C, respectively, at a heating rate of 10 °C min^{-1}, retained for 10 min, and then cooled in a Carbolite furnace (static air). The thus generated phases should be essentially similar to those formed at 300, 400, and 500 °C with TGA or DTA because of the similar heating routines applied. The XRD patterns of these furnace-heated samples are displayed respectively in parts a (400 °C) and b (500 °C) of Figure 6.

For the 300 °C heated samples, the XRD patterns are essentially similar to those of Figure 1, which indicates the layered structures of the samples are still maintained after heating. Nonetheless, significant differences can be found in the XRD patterns of 400 °C heated samples (Figure 6a). In particular, the (006) reflection, which corresponds to half of a basal spacing ($d_{003} = 2d_{006}$), has been severely broadened, shifting toward the higher side of 2θ. It is thus clear that the layered structures of these compounds had undergone serious destruction.[24] Actually, the dehydration of these samples up to 300 °C causes little effect on the layer destruction, as the basal spacing only decreases by less than 0.1 Å at 300 °C (Table 3). However, it has been compressed after calcination at 400 °C (decreasing by 0.3 to 0.8 Å, Table 3). Furthermore, a new peak (MA1 and MA2) or a broad shoulder (MA3−MA5) at $2\theta \approx 43°$ appears (Figure 6a). This peak, together with another new peak at $2\theta \approx 62°$, is well developed at 500 °C (Figure 6b). These new peaks, attributed to the freshly formed oxides,[1,10,12,13,20] are characteristic of a rock-salt-like phase (e.g., MgO type).[43] On the other hand, the relatively strong band at $2\theta \approx 36°$ in calcined samples MA3−MA5 does not exclude the formation of trace cubic spinel oxides. In fact, it has been recognized that in decomposed $Mg_{1-x}Al_x$-CO_3-HTlcs at least some Al^{3+} cations are located in tetrahedral sites formed by the oxygen, and due to the presence of tetrahedral Al^{3+} cations, the observed rock-salt-type XRD patterns can also been referred to as a spinel-like phase.[44,45] The broadness of the rock-salt-type reflections in Figure 6b indeed suggests lacking the ordered cation distribution in the resultant oxide phase, which is in line with the observation of diffusion of trivalent cations into the

(39) Mascolo, G.; Marino, O. *Miner. Magn.* **1980**, *43*, 619.
(40) Xu, Z. P.; Zeng, H. C. *J. Phys. Chem. B* **2000**, *104*, 10206.
(41) Xu, Z. P.; Zeng, H. C. *Chem. Mater.* **2000**, *12*, 3459.
(42) (a) Jackson, J. G.; Novichikhin, A.; Fonseca, R. W.; Holcombe, J. A. *Spectrochim. Acta Part B* **1995**, *50*, 1423. (b) L_vov, B. V.; Novichikhin, A. *Spectrochim. Acta Part B* **1995**, *50*, 1427. (c) Jackson, J. G.; Fonseca, R. W.; Holcombe, J. A. *Spectrochim. Acta Part B* **1995**, *50*, 1449. (d) L_vov, B. V.; Novichikhin, A. *Spectrochim. Acta Part B* **1995**, *50*, 1459.
(43) Powder Diffraction File Card No.45-0946 for cubic MgO.; Joint Committee on Powder Diffraction Standards, Swarthmore, PA, 1995.
(44) Reichle, W. T.; Kang, S. Y.; Everhardt, D. S. *J. Catal.* **1986**, *101*, 352.
(45) Rebours, B.; d'Espinose de la Caillerie, J. B.; Clause, O. *J. Am. Chem. Soc.* **1994**, *116*, 1707.

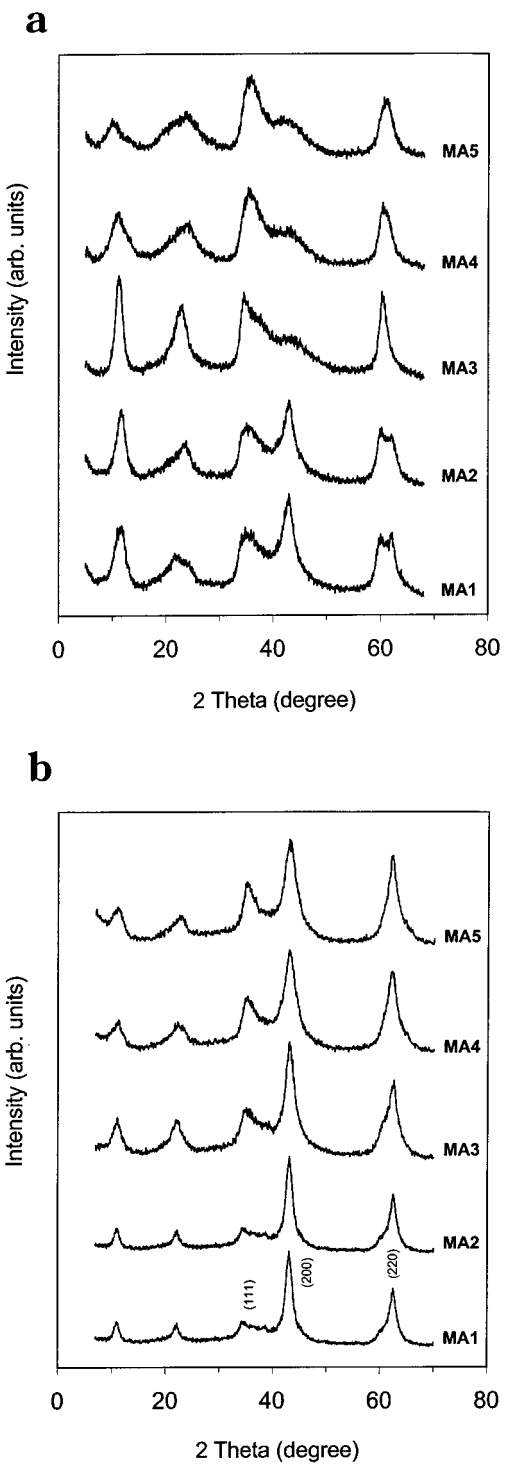

Figure 6. XRD patterns of calcined samples MA1−MA5 (a) at 400 °C and (b) at 500 °C for 10 min in static air (heating rate: 10 °C min^{-1}).

Table 3. Changes of Basal Spacing (d_{003} in Å) of the Studied $Mg_{1-x}Al_x$-NO_3-HTlcs with Heating Temperature

sample	as-prepared	calcined at 300 °C	calcined at 400 °C	calcined at 500 °C
MA1	8.13	8.09	7.7	8.0
MA2	8.08	8.02	7.7	8.0
MA3	8.49	8.48	7.8	8.0
MA4	8.95	8.84	8.1	7.9
MA5	8.94	8.84	8.6	8.0

tetrahedral sites when the $Mg_{1-x}Al_x$-CO_3-HTlcs decompose.[21]

It is worth noting that the basic layered structures of HTlcs still remain even after heated at 500 °C, although they are in a small quantity (suggested in Figure 6b). More interestingly, the condensation of the basal spacing becomes apparent; it reduces first from 8.08 to 8.95 to 7.7−8.6 Å at 400 °C and then uniquely to 7.9−8.0 Å at a higher heating temperature of 500 °C (Table 3). The small increases in the basal spacing observed in MA1−MA3 (500 °C heated) are attributed to the nitrate anion changing from a "flat-lying" position to a vertical standing position (see next subsection). Based on the TGA/FTIR results, we understand that the dehydroxylation has been almost completed at this temperature (Figure 5a), although there are still some nitrate anions remaining in the samples (Figure 5b). It is thus believed that the layered structures are constructed by partially dehydroxylated brucite-like layers (i.e., oxide-hydroxide layers) that are separated by mono- or bidentate NO_3^- anions. As shown in Figure 7a, the peak at 1384 cm^{-1} (ν_3 mode of NO_3^- with D_{3h} symmetry) is the most intense, indicating that most NO_3^- anions are still intercalated in these samples and in an unperturbed state even though the dehydroxylation has been close to completion in some cases (e.g., for MA1 and MA2). Simultaneously, several weak peaks or shoulders emerge, situated at 1513−1528, 1320−1350, and 1020 cm^{-1} in the spectra. These peaks are due to the symmetry lowering from D_{3h} to C_{2v} in some of the NO_3^- anions, i.e., from "free" to monodentate and/or bidentate NO_3^-.[32,46] From MA1 to MA5, the peak at 1513−1528 cm^{-1} (and similarly other C_{2v} peaks) becomes weaker and weaker, which indicates that it becomes more difficult for NO_3^- to change from D_{3h} to C_{2v} as x value increases; i.e., the crowdedness of anions increases. This finding has in fact supported our recent new models for nitrate arrangements in the interlayer space.[26] If they were tilt-lying in the interlayer at high x value, as suggested in other studies, the initial interlayer nitrate anions should have been more easily converted to C_{2v} and the intensities of vibrational peaks at 1513−1528 cm^{-1} should have shown an opposite trend to that shown in Figure 7a.

On the other hand, nitrate anions are almost gone at 500 °C and the remaining ones are largely in C_{2v} symmetry (Figure 7b). Considering the results found in the DTA (Figure 3a), DrTGA (Figure 3b), and the chromatogram of NO_2 (Figure 5b), we could make a postulation that, at 500 °C, NO_2 mainly comes from the intermediate metal nitrate species formed earlier. Therefore, the evolution peaks of NO_2 at 437, 467, and 449 °C for samples MA3, MA4, and MA5, respectively, should be ascribed to the direct decomposition of nitrate anions (in D_{3h} symmetry). As for samples MA1 and MA2, the above two ways of NO_2 release may be largely overlapped due to the smaller basal spacing, showing as an apparently continuous process (Figure 5b).

Decomposition Pathways. In light of the above findings, the decomposition of MgAl-NO_3-HTlcs can be divided into two major stages. In the first stage, dehydration occurs as follows:

(46) Schraml-marth, M.; Wokaun A.; Baiker, A. *J. Catal.* **1992**, *138*, 306.

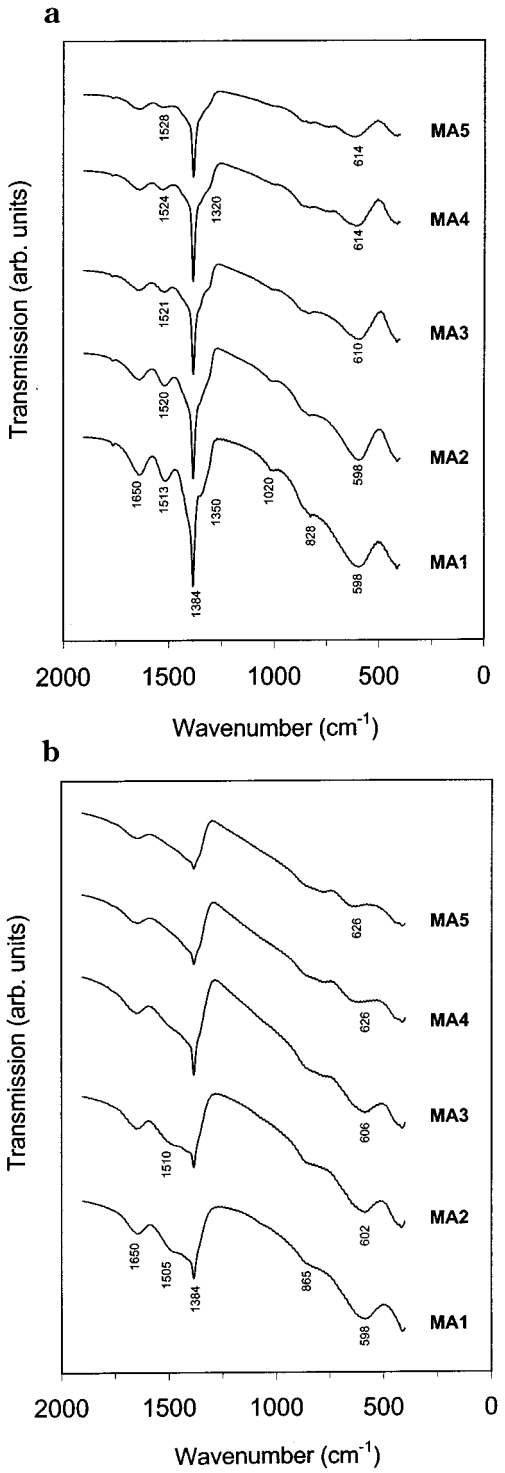

Figure 7. FTIR spectra of calcined samples MA1−MA5 (a) at 400 °C and (b) at 500 °C for 10 min in static air (heating rate: 10 °C min^{-1}). The spectra of 300 °C calcined samples (not shown) are almost identical to those of Figure 2.

$$Mg_{1-x}Al_x(OH)_2(NO_3)_x \cdot nH_2O \xrightarrow{50-150\ °C} Mg_{1-x}Al_x(OH)_2(NO_3)_x + nH_2O \quad (1)$$

Although most gaseous water escapes from the interlayer space, the basal spacing is not affected. In the second stage, two processes, i.e., both dehydroxylation and decomposition of NO_3^-, are involved. For samples MA1 and MA2, these two thermal reactions occur in sequence with only slight overlapping:

$$Mg_{1-x}Al_x(OH)_2(NO_3)_x \xrightarrow{300-380\ °C} Mg_{1-x}Al_xO(NO_3)_x + H_2O \quad (2a)$$

$$Mg_{1-x}Al_xO(NO_3)_x \xrightarrow{360-540\ °C} Mg_{1-x}Al_xO_{1+(x/2)} + xNO_2 + (x/4)O_2 \quad (2b)$$

The gaseous products NO_2 and O_2 are the same as those in the general decomposition of metal nitrates.[47] Note that O_2 is IR inactive and thus not observable in our TGA/FTIR experiments. For MA3−MA5, however, the mechanism of decomposition is much more complicated. A comparison of parts a and b of Figure 5 clearly shows a common signal respectively at 430 and 460 °C on both H_2O and NO_2 chromatograms. Since the hydrotalcite-like phase of MA3−MA5 is more difficult to be converted to the rock-salt structure (Figure 6), it is expected that the H_2O formed from retained hydroxyl groups will only be evolved together with NO_2 when the hydrotalcite structure is collapsed at a higher temperature. In our measurement conducted in air stream, the characteristic IR absorption of NO at 1904 cm^{-1} is not detected,[36,38] which can be attributed to lack of reducing reagents in the interlayer space or in the gas phase. Furthermore, it should be mentioned that the reaction 2b is quite different from the decomposition of some heavier metal nitrates. As reported in the literature, NO is also an important product in the decompositions of $Pb(NO_3)_2$, $AgNO_3$, hydrated $Cu(NO_3)_2$, and $Cd(NO_3)_2$ at a pressure of 3 x 10^{-7} Torr, where NO is formed through the catalytic decomposition of NO_2 over the in situ formed metal oxide catalysts.[42]

During the decomposition, the conversion of intercalated "free" NO_3^- to gaseous NO_2 has attracted considerable attention. In particular, we had recently proposed a mechanism to describe NO_3^- decomposition in a $Co_{1-x}^{II}Co_x^{III}$-NO_3-hydrotalcite-like compound.[41] First, NO_3^- may directly decompose to NO_2, leaving an anionic oxygen to attach the cobalt oxide or hydroxide layer. Second, NO_3^- may attach an anionic vacant site of the partially dehydroxylated brucite-like layers (or metal oxide-hydroxide) to form an intermediate metal nitrate species and then the intermediate decomposes to give off NO_2 gas and a metal oxide species.[41]

Figure 8 gives a schematic representation for the above discussed pathways. Interestingly, for the vertically standing metal nitrate species, the thickness of the partially dehydroxylated brucite-like layer is estimated to be 4.6 Å (the thickness of normal brucite-like layer is 4.8 Å), and the height of the nitrate anion including a van der Waals radius for the two end oxygen atoms is 3.3 Å (1.9 + 1.4 Å),[48] the sum of which will give an estimated basal layer distance of 7.9 Å, identical to our observed values (7.9∼8.0 Å, 500 °C, Table 3).

To understand these processes better, some particle size data and lattice parameters observed in this work are tabulated in Table 4. For the original brucite-like layers prior to thermal decomposition, the distance between two nearest neighboring octahedrons (the

(47) Stern, K. H. *J. Phys. Chem. Ref. Data 1* **1972**, 751.
(48) (a) *Handbook of Chemistry and Physics*, 80th ed.; Lide, D. R., Ed.; CRC: Boca Raton, FL, 1999; pp 9−11. (b) Kleinberg, J. B.; Argersinger Jr., W. J.; Griswold, E. *Inorganic Chemistry*; D. C. Heath and Company: Boston, 1960; p 356.

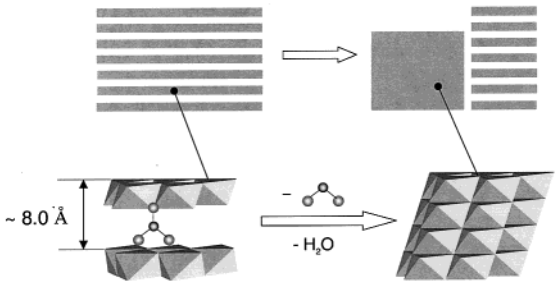

Figure 8. Schematic illustration for the interlayer condensation and topotactic transformation of hydrotalcite-like phase to rock-salt-like cubic phase based on the structural results of the present work.

Table 4. Particle Size and Lattice Parameters of the Structural Phases upon Heat Treatments

	as prepared		calcined at 400 °C		calcined at 500 °C		
sample	a,[a] Å	D_H,[b] nm	a,[c] Å	D_R,[d] nm	a,[c] Å	D_R,[d] nm	D_H,[b] nm
MA1	3.088	12.5	4.23	4.6	4.21	5.7	7.6
MA2	3.078	8.5	4.22	5.5	4.20	5.2	6.3
MA3	3.056	4.0[e]			4.20	5.1	5.6
MA4	3.046	9.0			4.21	4.3	4.3
MA5	3.040	10.9			4.21	4.0	4.7

[a] Lattice constant of brucite-like planes of $Mg_{1-x}Al_x$-NO_3-HTlcs.[26] [b] The dimension of particles in the *c*-axis of the hydrotalcite-like phase (fwhm's of (003) reflection were used in calculations). [c] Unit-cell constant of rock-salt-like phase, noting that the nearest distance between two oxygen octahedrons can be calculated from $(a^2/2)^{1/2}$. [d] The particle size of rock-salt-like phase (fwhm's of (200) reflection were used in calculations). [e] The minimum in MA3 is due to the change in configuration of nitrate anions in the interlayer space.[26]

nearest cation-to-cation distance) is about 3.088−3.040 Å in MA1−MA5 samples, owing to a gradual reduction in cation-to-cation repulsion with the increase of interlayer spacing or increase in the Al^{3+} content.[26] This distance is reduced slightly to 2.98−2.99 Å (MA1 and MA2, notes in Table 4) and further to 2.97 Å (MA1−MA5, notes in Table 4) when the samples are converted to rock-salt-like phase at 400 and 500 °C, respectively. The reduction is expected because some Al^{3+} cations may not be situated in the octahedral sites and more importantly the three-dimensional structure is formed after the thermal decomposition. The small contraction among the oxygen octahedrons indeed allows a smooth topotactic transformation of the brucite-like layers into the rock-salt-like structure when NO_2 molecules are released (Figure 8), noting that the topotactic transformation of the layered structures during the thermal decomposition have been observed in many HTlcs.[21,44,45,49,50]

According to the dimensional data reported in Table 4, it is known that the coherence length of the cubic closed packed oxygen network decreases from 57 to 40 Å in 500 °C heated samples when the trivalent content in the precursor HTlcs increases. This is understandable since any increase in Al^{3+} in the brucite-like layers would further differ the final chemical composition for the rock-salt-like MgO or randomness of cation distribution in the three-dimensional oxygen network. As for the small quantities of HTlc phases after the major dehydroxylation at 500 °C, the crystalline dimension along the *c*-axis still retains a similar trend as that in their initial HTlcs, although the variation is much gentler now due to the partial conversion to the rock-salt-like phase (Table 4). This observation indicates a strong link between the two phases and therefore further supports the topotactic transformation mechanism in the final oxide formation, as depicted in Figure 8.

Conclusions

In summary, thermal decomposition pathways of hydrotalcite-like compounds $Mg_{1-x}Al_x(OH)_2(NO_3)_x \cdot nH_2O$ ($x = 0.20-0.34$) vary with the contents of nitrate anions and trivalent Al^{3+} cations. It is revealed in this work that the dehydroxylation and decomposition of nitrate anions in the low x (0.20−0.22) samples occur sequentially, while the two processes in the high x samples proceed simultaneously. In good agreement with structural models proposed for this class of compounds, the dehydroxylation process in the higher x (0.30−0.34) samples can be further resolved into smaller steps. The dehydroxylation reactions depend strongly on both chemical environment of hydroxyl groups in the brucite-like layers and amount of nitrate anions in interlayer space. When more nitrate ions are intercalated (and thus more trivalent Al^{3+}), the thermal stability of layered structure becomes higher. It is found that the decomposition of nitrate anions (into NO_2 and O_2) in the low-x samples is a continuous process, whereas that in the high-x samples is a discrete one. Based on TGA/FTIR analysis, it is revealed that at 400 °C most nitrate anions are still retained in the interlayer space, although some of them have been converted from D_{3h} to C_{2v} symmetry and the dehydroxylation reaction in the low x samples has largely completed. At 500 °C, intercalated nitrate anions are largely removed and the remaining ones are mainly in C_{2v} symmetry with a standing configuration between the two dehydroxylated brucite-like layers. The nearest distance between two neighboring hydroxyl (or oxygen) octahedrons changes from 3.088 to 3.040 to 2.99−2.97 Å when the hydrotalcite-like phase is topotactically transformed to the rock-salt-like (MgO-like) phase at elevated temperatures.

Acknowledgment. We gratefully acknowledge research funding (R-279-000-064-112 and A/C50384) cosupported by the Ministry of Education and the National Science and Technology Board, Singapore. Z.P.X. thanks the Chemical and Process Engineering Center, National University of Singapore, for providing financial support for postgraduate study.

CM010347G

(49) (a) Petrov, K.; Markov, L.; Rachev, P. *Reactiv. Solids* **1987**, *3*, 67. (b) Markov, L.; Lyubchova, A. *J. Mater. Sci. Lett.* **1991**, *10*, 512.
(50) Chellam, U.; Xu, Z. P.; Zeng, H. C. *Chem. Mater.* **2000**, *12*, 650.